Journal of Power Sources 196 (2011) 801–807

Contents lists available at ScienceDirect

Journal of Power Sources

journal homepage: www.elsevier.com/locate/jpowsour

Development and application of an actively controlled hybrid proton exchange membrane fuel cell—Lithium-ion battery laboratory test-bed based on off-the-shelf components

V. Yufit, N.P. Brandon*

Dept. Earth Science and Engineering, Imperial College, London SW7 2AZ, UK

ARTICLE INFO

Article history:
Received 8 March 2010
Received in revised form 8 June 2010
Accepted 11 June 2010
Available online 22 June 2010

Keywords:
Fuel cell
Battery
Hybrid
Test bench

ABSTRACT

The use of commercially available components enables rapid prototyping and assembling of laboratory scale hybrid test-bed systems, which can be used to evaluate new hybrid configurations. The development of such a test-bed using an off-the-shelf PEM fuel cell, lithium-ion battery and DC/DC converter is presented here, and its application to a hybrid configuration appropriate for an unmanned underwater vehicle is explored. A control algorithm was implemented to regulate the power share between the fuel cell and the battery with a graphical interface to control, record and analyze the electrochemical and thermal parameters of the system. The results demonstrate the applicability of the test-bed and control algorithm for this application, and provide data on the dynamic electrical and thermal behaviour of the hybrid system.

1. Introduction

Fuel cells and rechargeable batteries combined with electric motors are increasingly seen as an alternative to hydrocarbon fuel and internal combustion engines to power vehicles designed to move on the ground, in the air, and on/under the water. However, fuel cell applications in vehicles are currently limited to demonstration vehicles, primarily due to cost concerns, while low energy density and capacity currently restrict batteries to short duration applications. Therefore, the hybridization of these two different electrochemical devices has been shown to most cost effectively meet the power and energy demand of a transport application [1]. There are two major options when designing such a hybrid system, namely either passive or active power sharing. The former is related to the direct connection of a fuel cell to a battery with the minimum possible number of electronic components, i.e. a voltage limiter to eliminate possible battery overcharging [2] and a diode to prevent fuel cell charging. Such a passive hybrid system has a number of advantages such as low complexity and higher efficiency compared to an active hybrid, however it requires precise voltage matching between the fuel cell and the battery. Another drawback of the passive hybrid system lies in the uncertainty of power sharing between the fuel cell and battery due to the dependence of the maximum power available on the state-of-charge of the battery.

These disadvantages can be eliminated by incorporating a step-up or step-down controllable DC/DC converter, which can be accomplished in one of two configurations; (1) the fuel cell is connected to the battery via a DC/DC converter while the battery is directly connected to the load, or (2) the fuel cell is directly connected to the load with the battery connected to the load through a DC/DC converter. It has been found experimentally that the former configuration is preferred [3], probably because of the slower response of the fuel cell in the latter configuration [4].

With proper voltage matching by a DC/DC converter, any combination of fuel cell and rechargeable battery can be used in an active hybrid system. For example, the proton exchange membrane (PEM) fuel cell can be combined with a lead acid [5], nickel/cadmium [6], nickel/metal hydride [7] or lithium-ion battery [3]. It has been also demonstrated that an active hybrid system is not limited to room temperature operation, being able to use high temperature electrochemical power sources such as a solid oxide fuel cell and a ZEBRA (molten $NaAlCl_4$) battery [8].

The crucial component of the active hybrid system is the DC/DC converter since it regulates the power shared between various components of the system and, unavoidably, reduces the total efficiency of the system. The efficiency of the DC/DC converter can be significantly improved by proper design, and may reach >90% [9].

This work addresses the integration and control of a commercially available battery pack, fuel cell system and DC/DC converter, allowing the dynamic system behaviour to be explored on a lab-

* Corresponding author at: Imperial College, Department of Earth Science and Engineering, Prince Consort Road, RSM Building, London SW7 2AZ, UK.
Tel.: +44 20 7594 5704.
E-mail address: n.brandon@imperial.ac.uk (N.P. Brandon).

0378-7753/$ – see front matter © 2010 Elsevier B.V. All rights reserved.
doi:10.1016/j.jpowsour.2010.06.029

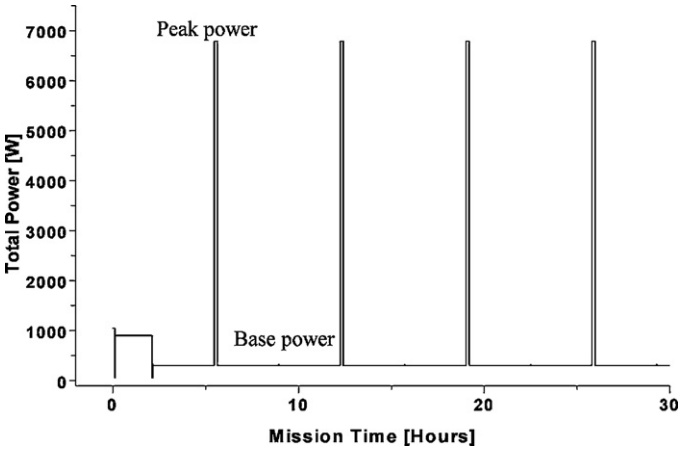

Fig. 1. Typical power profile for an unmanned underwater vehicle (UUV).

oratory test-bench as part of a study into the design of a hybrid fuel cell-battery system for autonomous underwater vehicle applications.

2. Experimental setup

2.1. Choice of components

The primary goal of designing and assembling of the test-bed was a need to test the power profiles [10] for an unmanned underwater vehicles (UUV). For this application the hybrid system must meet a maximum power of about 7 kW for 10 min, while the base power is not less than 0.3 kWe (Fig. 1). The proposed solution to this power demand is a Li-ion battery/hydrogen fuelled fuel cell hybrid. Most of the power (60–90%) during the pulse discharge is provided via the battery, with the fuel cell primarily acting as a battery charger. This configuration requires a relatively simple and small (compared to the battery and fuel cell size and weight) DC/DC converter with remotely regulated output voltage or (ideally) current.

In order to implement the power profiles for a UUV in a lab-scale hybrid system, the power demand was down scaled to 5% of its nominal value i.e. to a 350 W peak. A battery pack of seven $LiFePO_4$ cells (see Table 1) connected in series (7s1p topological configuration) was built to deliver the peak power demand. Every cell had an initial capacity of 10 Ah and allowed an operational discharge rate of 1.5–2 C (15–20 A). A PEM fuel cell system with a nominal maximum power of 100 W and a DC/DC converter with nominal output voltage of 28 V and maximum output power of 100 W were assembled to meet the base power demand.

2.2. Design of the system

A schematic diagram of the experimental hybrid fuel cell-battery system is given in Fig. 2. As seen from the figure, the PEMFC is connected to the programmable DC/DC converter via its control box. This fuel cell control device protects the fuel cell stack from overheating and power overloading, and regulates both the amount of hydrogen entering the fuel cell, and the amount of air blown to flow-channels (by increasing or decreasing the fan speed, which is also used for cooling the fuel cell stack).

In order for the H-100 fuel cell to operate according to manufacturer requirements, its control box must be permanently connected to the external power supply. Therefore, a small highly efficient (90%) auxiliary DC/DC step-down converter (Powergood) was introduced between the battery and fuel cell control box (P+, P− connections).

The programmable DC/DC converter output is connected directly to the battery and the load. By varying its output voltage

Table 1
Specification of individual components.

Component	Specifications	Manufacturer/supplier
Battery	Pack of 7 $LiFePO_4$ cells (10 Ah) in series. 2.8 kg, nominal output of 21 V.	Cyclone Taiwan
Fuel cell	Self-humidifying PEM FC system (H-100). 0.8 kg. Maximum rated power of 100 W. Operating voltage of 10–18 V (OCV).	Horizon Fuel Cell Technologies
DC/DC	Megamod chassis-mount (VI-200 series) step-up converter with broad input of 10–20 V and regulated output. Nominal voltage of 28 V and maximum output power of 100 W.	Vicor Power

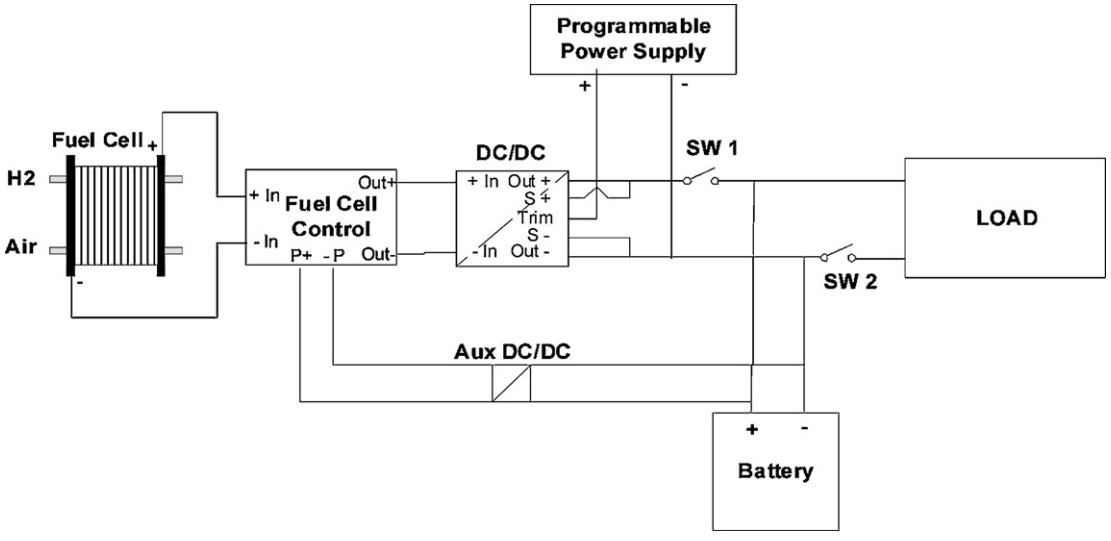

Fig. 2. Schematic illustration of the hybrid system.

with respect to that of the battery, it is possible to regulate the charging current flowing from the fuel cell. To do so, the trim lead (Trim) of the converter must be driven from a source referenced to the negative sense lead (S−), and kept in the range of 1.25–2.75 V, which corresponds to 14–31 V potential difference between leads (out −) and (out +) of the converter. The source could be any programmable power supply or data acquisition system equipped with an analog output module.

System parameters such as the voltage, current and temperature of the battery, fuel cell and DC/DC converters were simultaneously monitored and logged by a Yokogawa MX100 data acquisition system. A programmable 1 kW electronic load (Fideris FCTS EL 1000-55 V) operating in constant power mode was used to simulate the power demand of the actual load.

2.3. Design of control software

In order to ensure the autonomous operation of the whole hybrid system, LabView software was used to create a Virtual Instrument (*VI*) to control and monitor the parameters of the system. This could be compiled and implemented in a real time embedded system compatible with LabView, for example a Compact RIO (National Instruments).

The controlling *VI* monitors different parameters to ensure proper operation of the hybrid system. These parameters include battery voltage and current, temperature of every battery cell; fuel cell voltage and current; DC/DC converter input and output voltages and currents and temperature; auxiliary DC/DC converter input current. The values of battery power, energy, capacity and state of charge (SOC); fuel cell power; DC/DC input and output power and efficiency; auxiliary DC/DC input power are calculated by the same *VI* from the monitored parameters.

Since the DC/DC converter used in this work is equipped with programmable voltage output, it has the important task of controlling the *VI* to regulate current that flows from the DC/DC converter to the battery. Control of the DC/DC voltage output with respect to the battery controls the current flowing into the battery.

A simplified diagram of the controlling algorithm of the *VI* is presented is Fig. 3. The *VI* begins its operation with an initialisation of parameters with default values, switching off all relays and starting monitoring and data acquisition. On starting the fuel cell, the *VI* sets the output potential of the DC/DC converter equal to that of the battery, switches on the SW1 relay to connect the converter to the battery and initialises the software-implemented PID controller gains with pre-determined values. Then the *VI* starts the main loop where the software-based PID controller regulates the output current from the DC/DC converter by continually comparing this current with the target value, and then applying a potential between the trimming and negative sense pins (Fig. 2). In other words, the software PID controller accepts the target current as a setpoint and the DC/DC output current as a process variable, while its output or manipulated variable is an actual voltage applied on the DC/DC trim-sense pins. The controlling *VI* calculates the magnitude of the error which is a ratio of deviation between the target and DC/DC output currents to target current, and uses this value to select a suitable proportional gain for fine adjustment of DC/DC output voltage.

The capacity (Q_{battery}) and energy (E_{battery}) along with the SOC of the battery are calculated continuously in every iteration of the loop according to Eqs. (1a)–(3):

$$Q_n = \sum_{k=1}^{n} (I_{\text{out},k} - I_{\text{load},k})(t_k - t_{k-1}) \tag{1a}$$

$$Q_{\text{battery}} = Q_{\text{initial}} + Q_n \tag{1b}$$

$$E_n = \sum_{k=1}^{n} V_{\text{battery},k}(I_{\text{out},k} - I_{\text{load},k})(t_k - t_{k-1}) \tag{2a}$$

$$E_{\text{battery}} = Q_{\text{initial}} V_{\text{initial}} + E_n \tag{2b}$$

$$\text{SOC} = \frac{Q_{\text{battery}}}{Q_{\text{nominal}}} 100\% \tag{3}$$

where I_{out} represents the DC/DC output current, I_{load} represents the total load current, Q_{initial} and V_{initial} represents the initial capacity and voltage of the battery, respectively, Q_{nominal} represents the face plate capacity of the battery, V_{battery} represents the battery pack voltage, n represents the iteration number, and Q_n and E_n represents the cumulative capacity and energy, respectively.

As Fig. 3 suggests, on every iteration the *VI* checks the system parameters to intercept one of the following four major events and respond accordingly:

(1) If the battery voltage or SOC is lower than a certain minimal value, the *VI* will open the SW2 relay and prevent a battery overdischarge. The *VI* will close the relay only if the battery SOC is equal or higher than 60% (or any other defined value).
(2) If the DC/DC output voltage is higher than or equal to the battery maximum voltage, the PI controller switches immediately into a constant voltage charging mode. Thus it prevents overcharging of the battery.
(3) If the fuel cell current exceeds a defined maximum value, the *VI* will set the DC/DC output voltage to the battery minimum voltage and re-initialize the PI controller. This prevents fuel cell overload.
(4) If the temperature of any individual cell or the DC/DC converter exceeds a pre-set level, the *VI* will open all relays and shut down the system.

3. Results and discussion

The operation of the hybrid system was tested in constant power mode. In order to simulate this mode, the electronic load was programmed to discharge the system under high (P_1) and low (P_2) power at short (t_1) and long (t_2) period of times respectively. Fig. 4 shows the power profiles of total load and fuel cell (or power at DC/DC output) that were imposed on the hybrid system.

The high power spike (region (a) of Fig. 4) is due to an overshoot from the electronic load PID controller when attempting to supply the desired constant power. This overshoot can be reduced by ensuring that the electronic load operates in constant current mode. The region (d) on the graph demonstrates the battery charging mode switch from constant current to constant voltage.

The power profiles of Fig. 4 correspond to a system with a high degree of hybridization (DOH) [10]. The DOH of the hybrid system, and the power of the fuel cell that represents that DOH, can be calculated from Eqs. (4) and (5).

$$\text{DOH} = 1 - \frac{P_{\text{FC}}\gamma_{\text{DC/DC}}}{P_1} \tag{4}$$

$$P_{\text{FC}}\gamma_{\text{DC/DC}} \geq P_{1,2} = \frac{P_1 t_1 + P_2 t_2}{t_1 + t_2} \tag{5}$$

where γ is the efficiency of DC/DC converter, P_{FC} is the charge power provided by the fuel cell, P_1, t_1 is the high discharge (or load) power and its duration respectively, P_2, t_2 is the lower discharge power and its duration respectively, and $P_{1,2}$ is the average discharge power.

Using Eqs. (4) and (5) and the data from Fig. 4, the DOH of the hybrid system can be calculated to be 0.84 (Table 2).

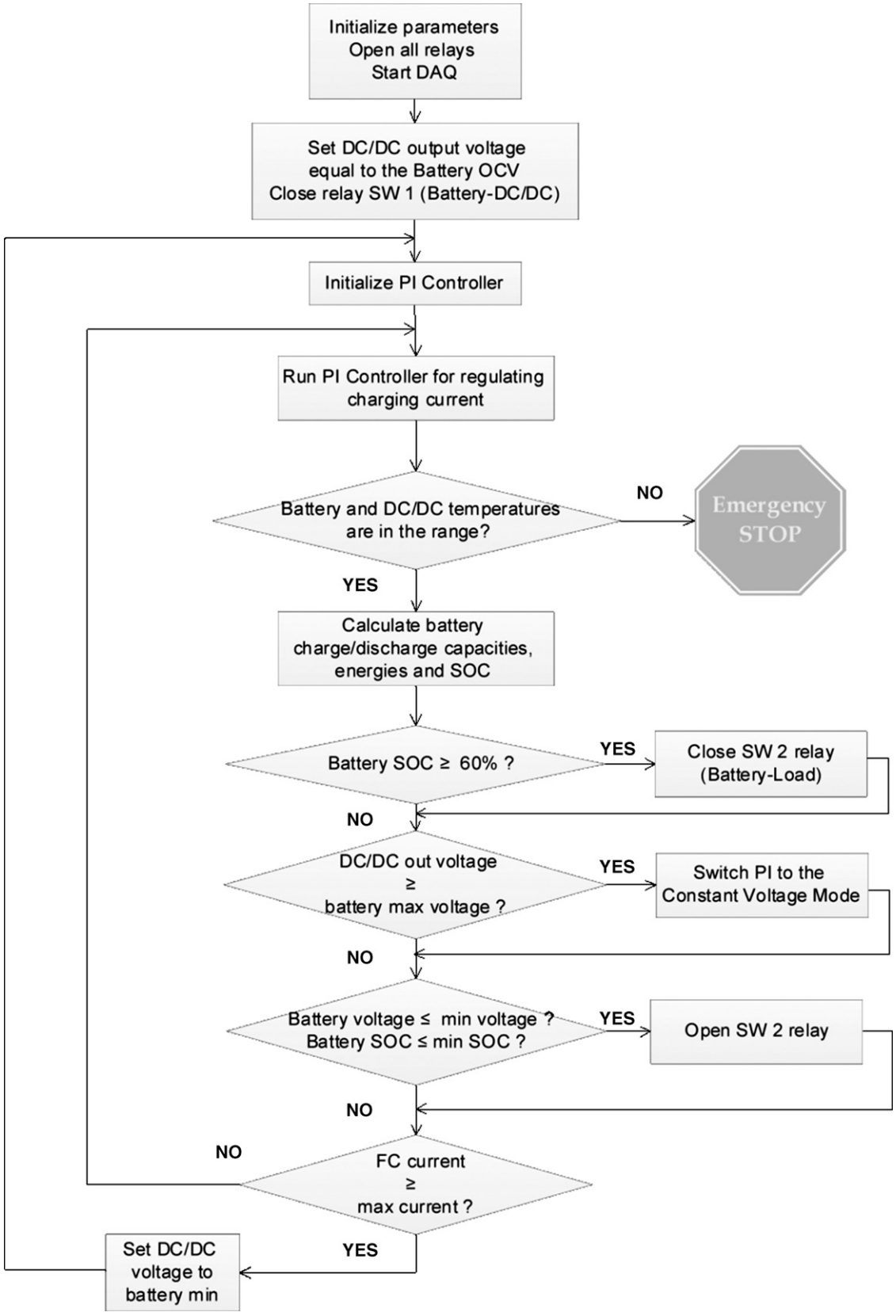

Fig. 3. Algorithm demonstrating how the controlling *VI* operates in real time.

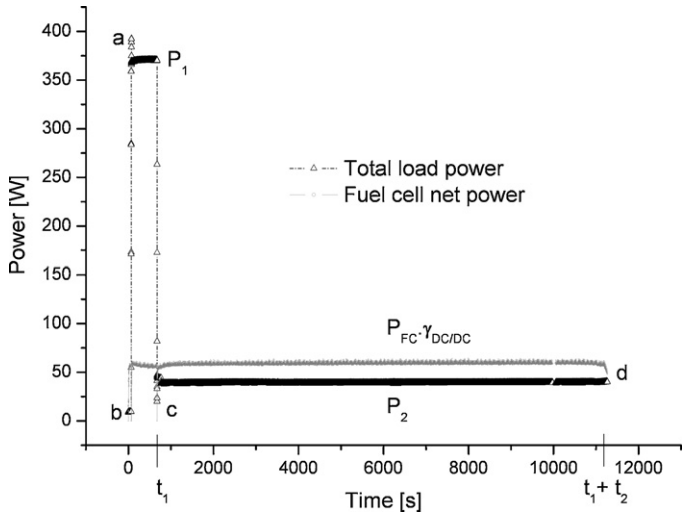

Fig. 4. Measured power profile of the tested hybrid system.

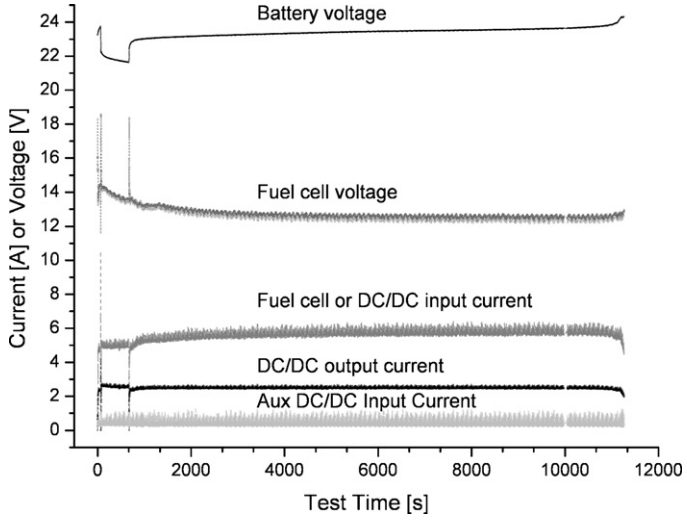

Fig. 5. Measured current–voltage response of the hybrid system.

Such a high DOH value indicates that the battery is the main source of power (84%) during the high pulse while the balance (16%) was supplied by the fuel cell. It is worth noting that the fuel cell was able to charge the hybrid system during the whole cycle except for very short periods at the beginning and end of the high pulse (Fig. 4, regions b–c).

Fig. 5 presents the measured voltage and current values of the battery, fuel cell and DC/DC converters during the whole operation period that correlates with the power profiles shown in Fig. 4. At the beginning of the test, the fuel cell current rose from 0 to 5 A which corresponds to 71 W, and was then kept at this level by the PI controller. When the high pulse occurred, the battery voltage decreased by few volts with regards to DC/DC converter output causing relatively high instantaneous increase in the current flowing from the fuel cell to the battery. When the controlling *VI* detected this increase in current, it trimmed down the DC/DC output to the battery minimum voltage, which was always less than the battery potential. Since the DC/DC converter response is relatively slow, it took about 30 ms to regulate the DC/DC output voltage. Once the DC/DC output voltage is trimmed down, the fuel cell current is then reduced to a minimum (there is always a 30 mA current flowing into the DC/DC converter) and the fuel cell voltage jumps to near its open circuit value, then the fuel cell current is slowly raised by the PI controller to its setpoint value (Fig. 6). On completing the high pulse, the battery voltage rises above the DC/DC output, and the fuel cell current drops off to a minimum value and gradually reaches the setpoint.

Hence, Fig. 6 shows that the PI controller was able to maintain a constant charging current of around 2.5 A through the whole operating period with only small fluctuations (6%) of the DC/DC output and slightly higher variations (12%) at the DC/DC input. These fluctuations are probably caused by a combination of power fluctuations in the electronic load, errors in the precision of trimming the DC/DC output voltage, and power oscillations of the fuel cell control unit. The latter is most likely to be the main cause of the fluctuations (shown in detail in Fig. 6) in the DC/DC current since the fuel cell control unit creates a closed-loop connection with the battery and programmable DC/DC converter.

In the hydrogen-air PEM fuel cell system with self-humidifying membrane, the necessary amount of oxygen is supplied by a rotating DC-powered blower. The higher the power supplied by the fuel cell the higher the rotation speed of the blower. This speed is regulated by the fuel cell control unit according to a pre-programmed algorithm which usually cannot be accessed and modified other than by the fuel cell supplier. The control unit also regulates the hydrogen supply and hydrogen purge by opening and shutting corresponding valves. The purge is necessary because it releases the hydrogen-depleted fuel to the atmosphere and allows fresh hydrogen to enter the cell. The fuel utilisation achieved within the fuel cell was relatively low at around 30% during these tests. Clearly this would need to be increased for technological applications, though this was not a focus during the study reported here. The operation of the purge valve is clearly seen in Fig. 6 as a small power spike taking place every 10 s.

Prolonged fuel cell operation under conditions of high power demand leads to an increase in fuel cell temperature. When the fuel cell control unit detects such a temperature rise, it will try to cool down the fuel cell by increasing the rotation speed of the blower which in turn results in higher power consumption for the blower, as well as higher fluctuations of current. Cooling of the fuel cell, initiated by the fuel cell control unit, can be detected by the increased fluctuation amplitude of the auxiliary DC/DC input current, when the output current of the programmable DC/DC converter drops to zero. The periodicity of these fluctuations is dependent on the fuel cell operation conditions and the control algorithm. The average power consumed by the control unit and the blower during operation – which also includes fuel cell cooling periods – is about 10 W and therefore cannot be neglected (this average value was taken into account when estimating the total load power Fig. 4).

Another important aspect of hybrid system operation is thermal behaviour. The H-100 fuel cell system was not equipped with any additional outputs for temperature monitoring, and thus the fuel cell temperature was not monitored during operation. However its temperature was constantly monitored by its control unit and this ensured proper fuel cell operation. In contrast to the fuel cell system, the battery pack did not have any built-in temperature control but its design was flexible enough to allow the attachment of a thermocouple to every cell so that the battery temperature could be monitored at 7 different points, and an average determined. Fig. 7 illustrates the battery thermal response during operation, as well as the corresponding battery voltage change. The battery temperature starts to rise immediately upon applying a high power

Table 2
Power values and degree of hybridization of the hybrid system.

P_1	t_1	P_2	t_2	P_{FC}	$P_{1,2}$	$\gamma_{DC/DC}$	DOH
370 W	603 s	39 W	1.05×10^4 s	71 W	57 W	0.84	0.84

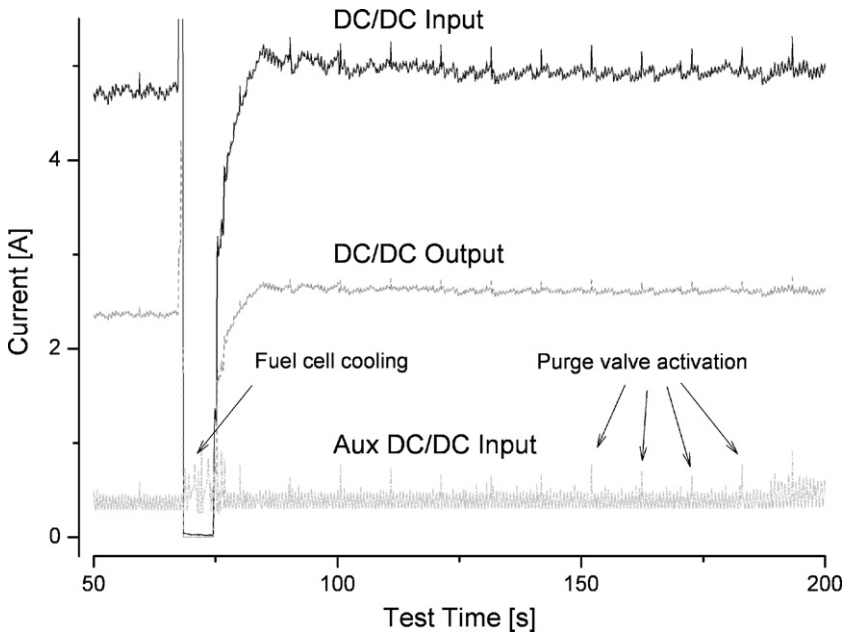

Fig. 6. Current fluctuations in the DC/DC converters during the first 3 min of operation.

pulse and reached a maximum which was 3 °C more than its initial temperature. Once the temperature reached a maximum, it remained at this level for about 2 min more on completion of the power pulse and then began to slowly decrease (battery cooling occurs only as result of natural convection in the battery used) to its steady-state value, which was 1 °C more then the initial battery temperature. Therefore both discharging and charging are responsible for temperature changes, but the rate and maximum values are dependent on the battery internal impedance, charge/discharge currents, charge/discharge times and the temperature of the environment within which the battery operates.

The battery temperature plays a crucial role in determining battery parameters such as capacity and cycle life over long term operation. Therefore it is important that the battery-fuel cell hybrid system be designed in such a way that the battery temperature never exceeds the maximum value set by the manufacturer, and that an appropriate thermal management strategy is in place during both steady state and transient operation.

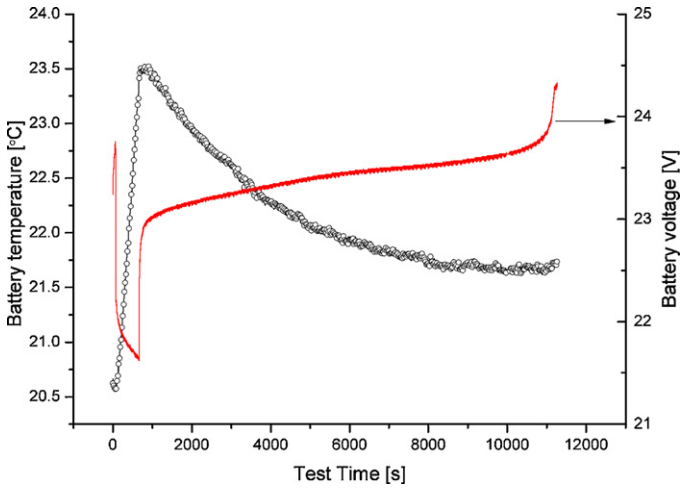

Fig. 7. Measured battery temperature and voltage during operation across the load cycle illustrated in Fig. 5.

4. Conclusions

This study has demonstrated that a lab-scale hybrid test-bed can be assembled from cost-effective off-the-shelf components without the additional design of specific hardware and low-level programming. A simple control algorithm was developed and implemented in LabView to regulate the current flow between the fuel cell and battery via a DC/DC converter with programmable output voltage. Preliminary testing of a Li-ion battery-hydrogen fuelled polymer electrolyte membrane fuel cell hybrid system representative of that needed for an unmanned underwater vehicle confirmed the effectiveness of the proposed control strategy for this application, and provided information regarding the dynamic operation of whole hybrid system.

It was demonstrated that, during operation of the system, the battery supplied most of the power during high pulse power demands while the fuel cell provided energy both for battery charging and low power load. It was also shown that the power demand of the fuel cell balance of plant cannot be neglected when sizing the hybrid system. Moreover, for the specific hydrogen-air fuel cell this power demand can be significant, particularly in the case when fuel cell control unit initiates cooling of the fuel cell while the fuel is under load. Unlike the fuel cell, the battery used did not enable thermal management and so its thermal behaviour is a matter of high importance. The battery generates heat during both charge and discharge. However, significant amounts of heat were generated during high discharge pulses. The battery therefore requires sufficient time to cool down between successive high power pulses, and this should therefore be taken into account in the overall hybrid system design and/or battery thermal design.

References

[1] G.J. Offer, D. Howey, M. Contestabile, R. Clague, N.P. Brandon, Energy Policy 38 (1) (2010) 24–29.
[2] P.B. Jones, J.B. Lakeman, G.O. Mepsted, J.M. Moore, Journal of Power Sources 80 (1–2) (1999) 242–247.
[3] L.J. Gao, Z.H. Jiang, R.A. Dougal, IEEE Transactions on Aerospace and Electronic Systems 41 (1) (2005) 346–355.
[4] Z.H. Jiang, L.J. Gao, R.A. Dougal, IEEE Transactions on Energy Conversion 22 (2) (2007) 507–515.

[5] P. Thounthong, S. Rael, B. Davat, I. Sadli, IEEE Power Electronics Specialists Conference, vols. 1–7, 2006, pp. 897–903.
[6] A. Nasiri, V.S. Rimmalapudi, A. Emadi, D.J. Chmielewski, S. Al-Hallaj, IPEMC 2004: The 4th International Power Electronics and Motion Control Conference, vols. 1–3, Conference Proceedings, 2004, pp. 491–496.
[7] H.W. He, J.P. Gao, Y.M. Zhang, American Control Conference 2008, Seattle, WA, Conference Proceedings, 2008, pp. 605–610.
[8] D.J.L Brett, P. Aguiar, N.P. Brandon, R.N. Bull, R.C. Galloway, G.W. Hayes, K. Lillie, C. Mellors, C. Smith, A.R. Tilley, Journal of Power Sources 157 (2) (2006) 782–798.
[9] Z.H. Jiang, R.A. Dougal, IEEE Transactions on Industrial Electronics 53 (4) (2006) 1094–1104.
[10] Q. Cai, D.J.L. Brett, D. Browning, N.P. Brandon, Journal of Power Sources 195 (19) (2010) 6559–6569.